Desalination and Water Treatment
www.deswater.com

doi: 10.5004/dwt.2022.28285

252 (2022) 98–107
March

Research on the optimal submergence depth of the surface aerator in an oxidation ditch by computational fluid dynamics method

J. Ding, W. Wei*, Y. Cai, X. Bai, Z. Deng, J. Sun, Sh. Shao

State Key Laboratory of Eco-Hydraulics in Northwest Arid Region of China, Xi'an University of Technology, Xi'an, Shaanxi 710048, China, Tel. +86 15289399259; email: JDing2020@126.com (J. Ding), Tel. +86 15596886263; email: wei_wenli@126.com (W. Wei), Tel. +86 15191913820; email: Yxicai@126.com (Y. Cai), Tel. +86 17629017302; email: X_Bai2020@126.com (X. Bai), Tel. +86 13036581019; email: ZDeng2020@126.com (Z. Deng), Tel. +86 15675521120; email: J_Sun2020@126.com (J. Sun), Tel. +86 13649204867; email: ShShao2018@126.com (Sh. Shao)

Received 24 September 2021; Accepted 5 February 2022

ABSTRACT

The effect of the submergence depth of surface aerator on the structure of flow field, aeration gas-volume-fraction distribution, and the ability to move fluid in an oxidation ditch (OD) was studied by using an experimentally validated computational fluid dynamics model (in FLUENT6.3.26). The gas–liquid two-phase model with the three-dimensional (3D) renormalized group k–ε turbulence model was used to describe the gas–liquid two-phase flows in ODs; the pressure-implicit with splitting of operators algorithm was used to solve the velocity and pressure; and the volume of fluid method was used to simulate the water surface. The concept of the submergence depth ratio was introduced to describe the submergence depth of the surface aerator in the OD. With the different submergence depth ratios of 1/4, 1/3, 1/2, and 3/4, the velocity fields and gas content distributions were computed, by which the optimal submergence depth ratio from 1/3 to 1/2 of the surface aerator was obtained. The research result has a certain reference for reducing sludge deposit and prolonging liquid-gas mixing time in an OD.

Keywords: Oxidation ditch; Numerical simulation; Optimal submergence depth; Surface aerator

1. Introduction

Oxidation ditch (OD) is a kind of activated sludge process, also known as circular aeration tank. Its better mixture property makes the sewage treatment capacity be higher than that of other biological treatment methods; therefore, OD plays an important role in the city sewage and industrial wastewater treatment system. The studies on ODs in all aspects at present have achieved lots of results [1–3], which are mainly in the process design and equipment improvement, the simulation and test research on flow hydraulic characteristics, and the biological reaction kinetics.

In order to test the effects of the improved surface aerators in an OD, Li et al. [4] performed a comparative study on the dissolved oxygen before and after the improvement of surface aerators. Li et al. [5] measured the velocity field of an OD model by the acoustic Doppler velocimeter (ADV), by which the mathematical expressions for the change of velocity in the straight ditch were obtained. Yang et al. [6] discussed the influence of the installation position and the submerged depth of surface aerators on the distribution of dissolved oxygen concentration in an OD. Lei et al. [7] proposed a 3D three-phase fluid model for the simulation of water-gas, water-sludge, and gas-sludge interactions to obtain the distribution of hydrodynamics,

* Corresponding author.

oxygen mass transfer, carbon oxidation, nitrification and denitrification in an OD. Xie et al. [8] proposed a two-phase liquid-solid computational fluid dynamics (CFD) model with the Takács double exponential sedimentation velocity function for the simulation of flow field and sludge settling in a full-scale Carrousel OD. Dang and Zhang [9] analyzed the effect of guiding plate on the hydraulics of an actual OD, which shows that the guiding plate can improve the transfer efficiency of oxygen, increase the oxygenation capacity of surface aerators, and also can improve the velocity distribution of the upper and the bottom of the OD. Chen et al. [10] adopted the multiple reference frame (MRF) model to numerically simulate the 3D flow field in an OD with surface aerators under two conditions: with and without single diversion wall. Wei et al. [11] proposed a numerical method for the flow fields of OD, by which the longitudinal velocities along the representative vertical lines were simulated under working conditions of an Orbal OD, and the simulated results are in an agreement with the experimental ones.

At present, energy consumption from sewage treatment in China is great, which hinders the construction and operation of urban sewage treatment plants to a certain extent. In the activated sludge treatment system, the energy consumption produced by aeration turntable accounts for about 70% of that by the whole sewage treatment plant. Surface aerators of an OD have an important influence on the flow velocity and gas content distributions. The change of the rotation speed, submergence depth, and size of the surface aerators can affect the velocity and gas-content distributions. Some scholars have done the research on the surface aerators, but there are few studies on the simulation of the influence of submergence depth of surface aerators on the velocity field and gas content distributions in ODs; therefore, the main aim of this paper is to numerically solve the two-phase gas–liquid model with the 3D renormalized group (RNG) k–ε turbulence model for the simulation of an OD with different submergence depths of surface aerators. By comparing the simulated flow velocity and gas-content distributions of the OD, the optimal range of submergence depth of the surface aerator was obtained, which can effectively improve the OD flow velocity and gas content distribution so as to reduce sludge deposition at the ditch bottom and to prolong the mixing time of water and gas. Therefore, the results will have a certain guiding significance for the optimal design of ODs.

2. Materials and methods

2.1. Mathematical model

2.1.1. Governing equations

The 3D continuity equation and the Reynolds-averaged Navier-Stokes momentum equations that govern unsteady, compressible flows can be written as [11,12]:

Continuity equation:

$$\frac{\partial \rho}{\partial t} + \frac{\partial \left(\rho u_i\right)}{\partial x_i} = 0 \tag{1}$$

Momentum equation:

$$\frac{\partial \left(\rho u_i\right)}{\partial t} + \frac{\partial \left(\rho u_i u_j\right)}{\partial x_j} = -\frac{\partial p}{\partial x_i} + \frac{\partial}{\partial x_j}\left[\mu\left(\frac{\partial u_i}{\partial x_j} + \frac{\partial u_j}{\partial x_i}\right)\right] - \frac{\partial}{\partial x_j}\left(\rho\overline{u_i' u_j'}\right) + \rho g_i \tag{2}$$

where ρ is the density; t is time; x_i is the space coordinate in i-direction; p is the pressure; μ is the molecular kinematic viscosity; u_i and u_i' are the velocity and fluctuating velocity component in i-direction, respectively; g_i is the gravitational acceleration in i-direction; and the subscripts i, j = 1, 2, 3.

The turbulence stress term $-\rho\overline{u_i' u_j'}$ is computed from [11,12]:

$$-\rho\overline{u_i' u_j'} = \mu_t\left(\frac{\partial u_i}{\partial x_j} + \frac{\partial u_j}{\partial x_i}\right) - \frac{2}{3}\left(\rho k + \mu_t \frac{\partial u_i}{\partial x_i}\right)\delta_{ij} \tag{3}$$

and μ_t in Eq. (3) is the kinematic viscosity, and can be determined by the following formulas [11]:

$$\mu_t = \rho C_\mu \frac{k^2}{\varepsilon} \tag{4}$$

where k is turbulent kinetic energy; and ε is kinetic energy dissipation rate; C_μ is a constant.

The RNG k–ε turbulence model is used for the closure of momentum Eq. (2), given as [11,12]:

k-equation:

$$\frac{\partial \left(\rho k\right)}{\partial t} + \frac{\partial \left(\rho k u_i\right)}{\partial x_i} = \frac{\partial}{\partial x_j}\left[\left(\mu + \frac{\mu_t}{\sigma_k}\right)\frac{\partial k}{\partial x_j}\right] + G_k - \rho\varepsilon \tag{5}$$

ε-equation:

$$\frac{\partial \left(\rho \varepsilon\right)}{\partial t} + \frac{\partial \left(\rho \varepsilon u_i\right)}{\partial x_i} = \frac{\partial}{\partial x_j}\left[\left(\mu + \frac{\mu_t}{\sigma_\varepsilon}\right)\frac{\partial \varepsilon}{\partial x_j}\right] + C_1 \frac{\varepsilon}{k} G_k - \rho C_2 \frac{\varepsilon^2}{k} \tag{6}$$

where C_μ, σ_k, C_2 and σ_ε are the empirical constants and have a value of 0.085, 0.7179, 1.68, and 0.7179, respectively; and other parameters are: $C_1 = 1.42 - \eta(1 - \eta/\eta_0)/(1 + \beta\eta^3)$, $\eta = Sk/\varepsilon$, $S = (2S_{ij}S_{ij})^{1/2}$, $\eta = 4.34$, $\beta = 0.015$, $S_{i,j} = \frac{1}{2}\left(\partial u_i/\partial x_j + \partial u_j/\partial x_i\right)$.

2.1.2. Volume of fluid method

The volume of fluid (VOF) method [11,12] is used to describe the liquid/gas interface. The volume of water inside a cell is computed by $V_w = F_w \times V_c$, where V_c is the volume of the cell; V_w is the volume of liquid in the cell, and F_w is the volume fraction of liquid, representing the ratio of the volume occupied by liquid to the total volume of the control cell, with a range from 0 to 1. $F_w = 1$ represents a cell completely filled with liquid, $F_w = 0$ represents a cell completely filled with gas, and $0 < F_w < 1$ represents the liquid/gas interface.

According to the concept of VOF, we know that the gas volume fraction, F_g, represents the ratio of the volume occupied by gas, V_g, in a control cell to the total volume of the control cell, V_c, with a range from 0 to 1; and $F_w + F_g = 1$.

The liquid volume fraction, F_w, can be determined by solving a separate passive transport equation as:

$$\frac{\partial F_w}{\partial t} + \frac{\partial \left(F_w u_i\right)}{\partial x_i} = 0 \tag{7}$$

The physical properties of mixture, ρ and μ, in a computational cell, are computed from those of water and gas in accordance with the values of F_w and F_g:

$$\rho = F_g \rho_g + F_w \rho_w \tag{8}$$

$$\mu = F_g \mu_g + F_w \mu_w \tag{9}$$

where ρ_g and μ_g are the density and viscosity of gas, respectively; ρ_w and μ_w are the density and viscosity of water, respectively.

2.2. Computational region

The 3D computational region and the detail size of the model are shown in Fig. 1a and b, respectively. The testing physical model for the OD consists of two straight channels and two bends, and each straight channel has a width of 9.5 m and a length of 26 m, and each bend has a radius of 9.5 m. The submerged impeller was installed at the center of the left-hand bend, consisting of 8 blades with a thickness of 12.5 mm, a length of 1.132 m and a height of 0.5 m; the distance from the center of submerged impeller to the left-hand end of the intermediate baffle is 2.6 m, and the bottom surface of the submerged impeller is 1.0 m away from water surface. The surface aerator with a radius of 1.5 m consists of 19 discs with a thickness of 12.5 mm, and the spacing between the adjacent discs is 0.5 m; and the surface aerator was installed at the middle of the straight channel.

2.3. Grid generation

The grid was generated by the GAMBIT software [13], and the combination of structured and unstructured grids was adopted. The thickness of discs and blades is 12.5 mm, which shows that the thickness is very small compared to the size of the calculation region of the OD, therefore, it is simplified as an infinitely small one so as to generate a high quality grid. In another words, it is simplified as a two-dimensional (2D) problem with some boundary conditions. The total number of elements of the 3D grid is 268875. Fig. 2a–c show the 2D plane grid, 3D grid, and the local grid of the OD, respectively.

2.4. Initial and boundary conditions

The inlet and outlet boundary conditions have a little influence on the flow field of OD, so they were ignored in the numerical calculation. The initial conditions are that the initial water depth was given as 4.24 m and the initial velocity was set zero in the OD. Boundary condition at the top surface of the computational region was given a relative pressure of 0, and at the side walls and the bottom plan was given by the wall-function. The free surface was simulated by the VOF method. The motion of the submerged impeller and surface aerator relative to the OD was described by the MRF model with a sliding mesh method. The surface aerator runs at a speed of 2.5 rad/s, and the submerged impeller runs at a speed of 3.03 rad/s.

The MRF method in FLUENT6.3.26 is used to simulate the rotation movement, and the calculation domain is divided into three parts: the two rotation domains and the stationary domain. The calculation regions around the underwater impeller and the surface aerator are taken as the two rotation domains, and the other part is taken as the stationary domain, the grids for which are generated separately.

3. Definition of the submergence depth ratio of the surface aerator

The submergence depth of surface aerators of an OD has an important influence on the surface aeration capacity, flow movement, and the gas content and velocity distributions. When studying the optimal submergence depth of surface aerators, we introduced a dimensionless number called the "submergence depth ratio of the surface aerator", which was defined as the ratio of submergence depth h to diameter D of the surface aerator, as shown in Fig. 3.

In the simulations, to obtain the optimal submergence depth of the surface aerator, we made the size and the rotating speed of the surface aerator, and the initial and boundary conditions be the same, and we only changed the submergence depth of the surface aerator. We numerically simulated the flow velocities and gas contents under the 4 different submergence depth ratios, 1/4, 1/3, 1/2, and 3/4 of the surface aerator. The height of the axis

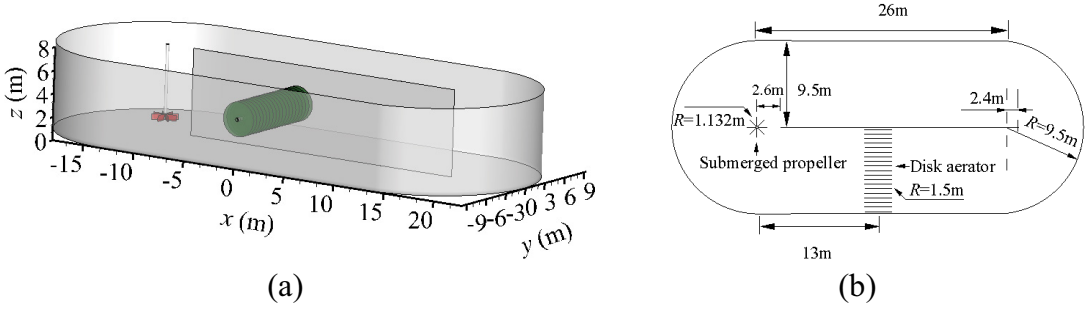

Fig. 1. Computational region: (a) 3D region and (b) detail size.

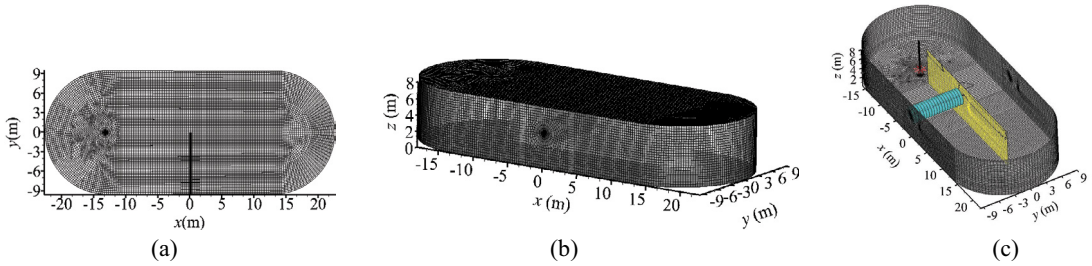

Fig. 2. Grids of the computational region: (a) 2D plane grid, (b) 3D grid, and (c) local grid.

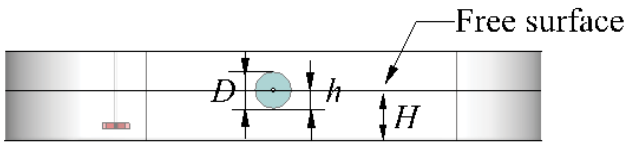

Fig. 3. Submergence depth of the surface aerator.

of the surface aerator to the ditch bottom corresponding to the 4 working conditions are 3.49, 4.24, 4.74, and 4.99 m, respectively, as shown in Table 1.

Table 1
Submergence depth ratios of the surface aerator

Submergence depth ratios (h/D)	Height of the axis of the surface aerator to the ditch bottom (m)
1/4	4.99
1/3	4.74
1/2	4.24
3/4	3.49

4. Results analysis

4.1. Flow field structures

Fig. 4a–d show the simulated streamlines on the horizontal plane at z = 1 m of a vertical distance to the ditch bottom, under the 4 different submergence depth ratios 1/4, 1/3, 1/2, and 3/4 of the surface aerator. The bends at two sides of the OD make the flow produce circulations in the straight channels. The existence of the circulation areas will cause sludge phase retention, and is unfavorable to the operation of the OD.

The submergence depth of the surface aerator greatly affects the flow fields in the OD. Fig. 4a and b show that, when the submergence depth ratio of the surface aerator is h/D = 1/2 or 1/3, the backflow area in the straight channel is smaller and the streamline distribution is more uniform, especially when the submergence depth ratio is h/D = 1/3, the circulation area is the smallest and the streamline distribution is the most uniform. Because of the inertia force at the bends, the velocity distributions at the exit sections of the bends are not uniform, which leads to the formation of circulation zones. Fig. 4c and d show the flow field distribution with the surface aerator at the submergence depth ratio of h/D = 1/4 and 3/4,respectively, which shows that when the submergence depth ratio is h/D = 1/4, there are large circulation zones in the two straight channels, and the existence of the circulation zones will cause sludge phase retention; when the submergence depth ratio of surface aerator is h/D = 3/4, the straight channel with the surface aerator also has a large circulation zone, and the flow field distribution is not uniform, which is not conducive to improving the sewage treatment efficiency of the OD.

In order to more clearly and comprehensively reflect the influence of submergence depth of surface aerator on the flow fields in the OD, the simulated streamline distributions on a cross-section of x = 5 m downstream of the surface aerator under the 4 working conditions are plotted, as shown in Fig. 5a–d, the left half of which (y < 0) is the streamline distribution in the straight channel without surface aerator; the right half of which (y > 0) is in the straight channel with surface aerator. From Fig. 5a and b, it shows that, when the submergence depth ratio is h/D = 1/2 or 1/3, the obvious flow mixing phenomenon appears in the cross-section of the straight channel with the surface aerator. The surface flow with higher energy mixes with that of lower energy, transferring energy to the middle and bottom flow in the straight channel, instead of directly transferring energy near water surface, which makes the energy distribution in the OD more obviously reasonable and accelerates the transfer of oxygen and prolongs the mixing time of water and air, so that the aeration capacity of the surface aerator can be improved. In Fig. 5c, there is no obvious flow mixing phenomenon because of the smaller submergence depth ratio, 1/4, of the surface aerator; Fig. 5d shows a more obvious mixing phenomenon than Fig. 5c, but its mixing effect is smaller than that of Fig. 5a and b.

Therefore, from the flow field distributions on the horizontal plane in Fig. 4a–d and on the cross-section in Fig. 5a–d, we made a conclusion that, when the submergence depth ratio of the surface aerator is h/D = 1/2 or 1/3, the flow field structure in OD can be improved and the operation of OD is better.

Resulting from the action of the underwater impeller and the surface aerator, the stable water surfaces of flows appear in the OD, as shown in Fig. 6a–d with the 4 different submergence depth ratios, 1/4, 1/3, 1/2, and 3/4, of the surface aerator. There is water on the surface aerator above the water surface because of the viscosity and the force of inertia of water.

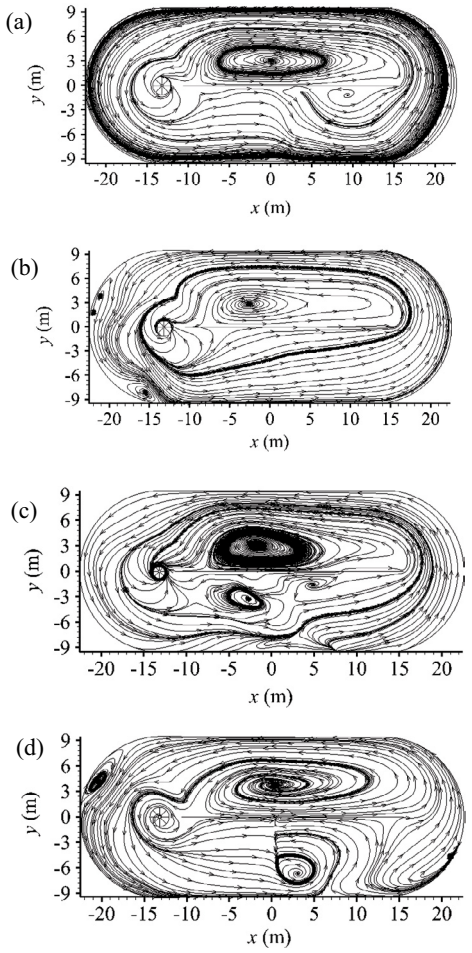

Fig. 4. Computed streamlines on the horizontal plane with the 4 different submergence depth ratios: (a) h/D = 1/4, (b) h/D = 1/3, (c) h/D = 1/2, and (d) h/D = 3/4.

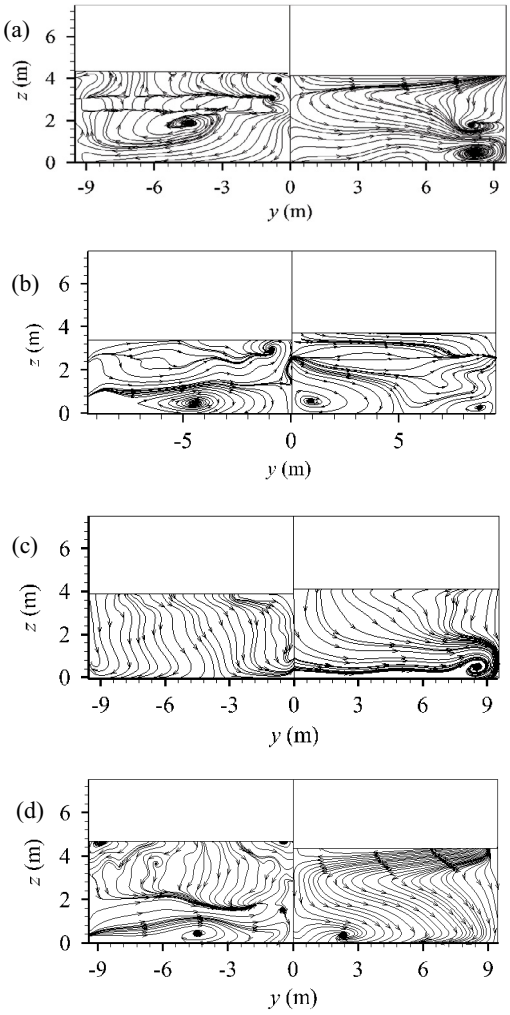

Fig. 5. Computed streamlines on the cross-section with the 4 different submergence depth ratios: (a) h/D = 1/4, (b) h/D = 1/3, (c) h/D = 1/2, and (d) h/D = 3/4.

4.2. Velocity distributions along water depth under the 4 different submergence depth ratios

The submergence depth of surface aerator of an OD has an important influence on the velocity distribution along water depth. In order to observe and analyze the velocity distribution along the water depth more obviously, the velocity distributions along the vertical lines at the 4 points shown in Fig. 7 were drawn in Fig. 8a–d, in which v represents the total velocity at a point in the space. Fig. 7 shows the position points 1–4 of the 4 vertical lines, and Table 2 shows the coordinates of the 4 point.

When studying the optimal submergence depth of the surface aerator, we fixed other factors as a constant in the simulation, such as: the aerator' size and rotating speed, and the initial and boundary calculation conditions; we only changed the submergence depth ratios of the surface aerator among 1/4, 1/3, 1/2, and 3/4.

With the submergence depth ratio of 1/4, both in the straight channel and in the bend ditch, upper and lower velocities along water depth are smaller than those of other submergence depth ratios, which shows that the submergence depth ratio of 1/4 cannot result in high flow velocity.

Table 2
Point coordinates of the vertical lines

Point	1	2	3	4
x (m)	14.2	19	14.2	6.77
y (m)	4.75	0	–4.75	–4.75

With the submergence depth ratio of 1/3, either in straight or in curved region, compared with the other submergence depth ratios, along water depth the velocity near bottom ditch increases, and near the water surface decreases, which shows that the flow tends to be uniform. The flow pattern is conducive to improving the processing ability of the OD, and to reducing sludge deposition at OD bottom. With the submergence depth ratio of 1/2, both in the straight and bend ditch, along water depth the velocity of upper flow is very big, but of lower flow is small, especially in the straight channel, that is, for lines 3–4, the ditch bottom velocity is less than 0.2 m/s, but the upper flow is larger,

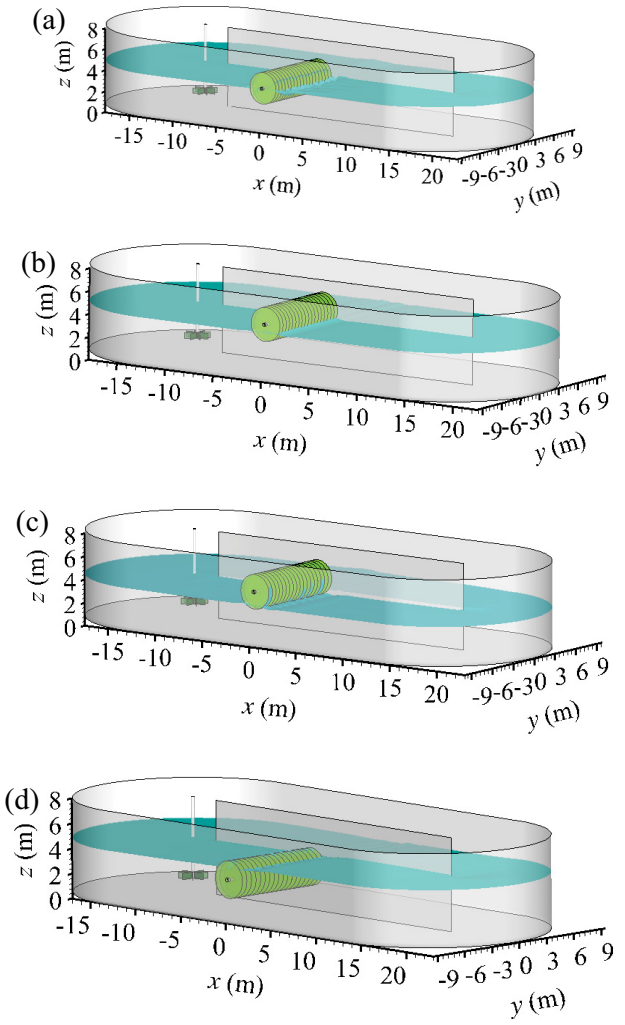

Fig. 6. Simulated water surface under the 4 different submergence depth ratios: (a) h/D = 1/4, (b) h/D = 1/3, (c) h/D = 1/2, and (d) h/D = 3/4.

up to 1.0 m/s. The difference of velocity between the upper and lower flows is great, which shows the uniformity of the total flow along the vertical direction is not good. With the submergence depth ratio of 3/4, in the straight and bend ditch, along water depth the upper flow velocity is nearly the same as that of the submergence depth ratio of 1/2, but the ditch bottom velocity is much smaller, which can easily lead to the sludge deposition near the OD bottom.

As analyzed between the 4 submergence depth ratios, we obtained that the submergence depth ratio of 1/2 is the most useful to drive the liquid to move in the OD.

4.3. Gas volume fraction distributions under the different submergence depth s of the surface aerator

The surface aerator drives fluid to move, and also aerates water flow in the OD. Therefore, the submergence depth of the surface aerator has an important function of aeration capacity. In order to compare the aeration capacity of surface aerator under different submergence

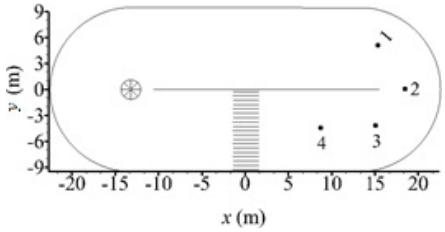

Fig. 7. Position points of vertical lines.

depths, the gas volume fraction distribution along the vertical lines at the 4 points (as shown in Fig. 7) were plotted under the different submergence depths of the surface aerator, as shown in Fig. 9a–d.

Fig. 9a–d show that, under the 4 submergence depth ratios of the surface aerator, either in the straight or in the curved region, gas volume fraction shows an increasing trend along the 4 vertical lines; the closer to the water surface, the greater is the gas volume fraction, and the maximum is of 0.7; the closer to the ditch bottom, the smaller is the gas volume fraction, and at the bottom it is close to 0.

With the submergence depth ratios of 3/4, 1/2, and 1/4, the gas volume fraction at the lower and upper parts along the 4 vertical lines was higher than that of the submergence depth ratio of 1/3, and the gas volume fractions have little difference between the submergence depth ratios of 3/4, 1/2, and 1/3.

Therefore, only from the angle of aerating capacity of the surface aerator, the submergence depth ratio of 1/3 is the most conducive one to improving the gas content of the upper and lower regions of the OD.

In order to have a better insight into these values of the velocity and the gas volume fraction, the calculated velocity and gas volume fraction distribution diagrams on the horizontal plane at z = 2.6 m are shown in Fig. 10a and b, from which we can clearly see the distributions of the velocity value and the gas volume fraction value.

When the underwater impeller rotates, the water around the underwater impeller rotates, as shown in Fig. 10a. Then, as shown in Fig. 10b, the rotating water above the underwater impeller drives air above the water surface into the water body, and the gas and water are mixed and form a gas–liquid mixture in motion in the OD. Therefore, above the underwater impeller, the value of gas volume fraction on the plane at z = 2.6 m is the largest, between 16% and 20%. When the surface aerator rotates, the air above the water surface is driven into the water body, and the gas and water are also mixed and form a gas–liquid mixture in motion; which makes the value of gas volume fraction on the plane at z = 2.6 m below the surface aerator be the largest, between 18% and 20%. In other areas, the value of gas volume fraction is relatively uniform, between 10% and 16%.

4.4. Analysis of the statistic velocity and the gas volume fraction for the OD

In order to prevent sludge deposition at ODs, the designing specification requires that the mean velocity over cross-section is greater than 0.3 m/s [12,13]. The values of

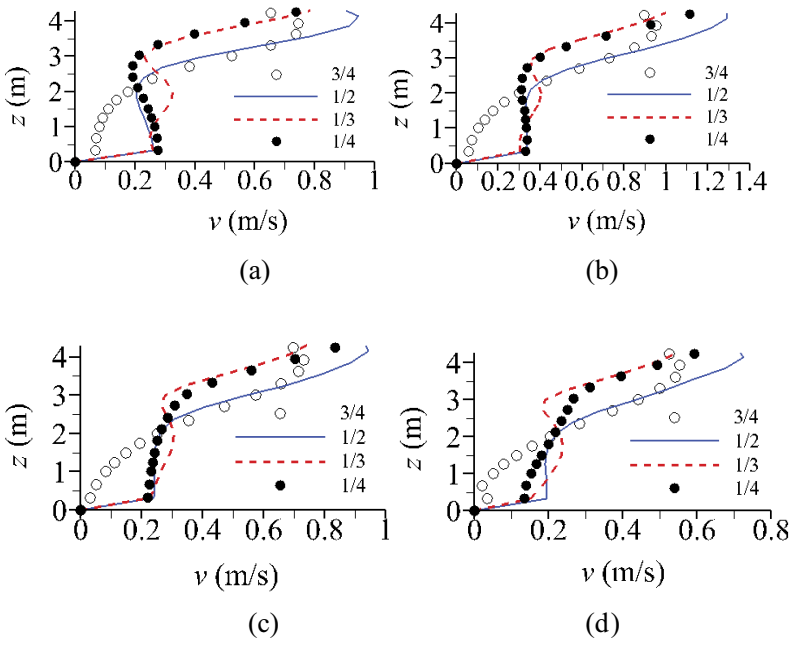

Fig. 8. Velocity distributions along the 4 vertical lines: (a) vertical line 1, (b) vertical line 2, (c) vertical line 3, and (d) vertical line 4.

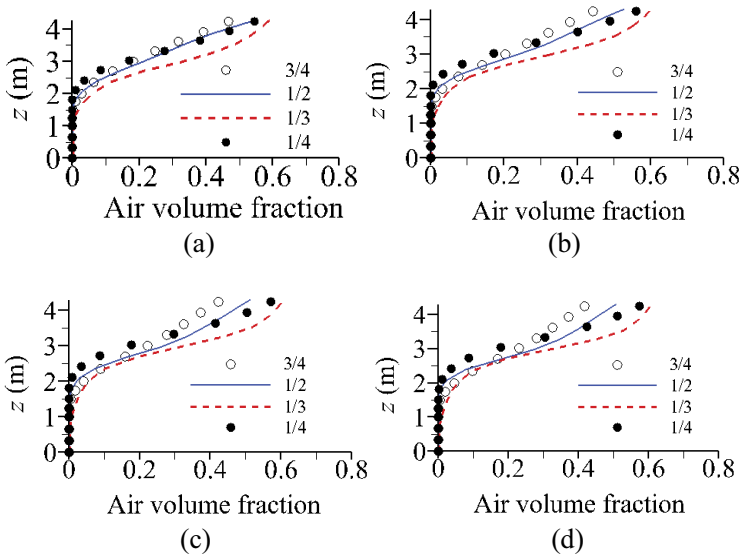

Fig. 9. Air volume fraction distributions along vertical lines: (a) vertical line 1, (b) vertical line 2, (c) vertical line 3, and (d) vertical line 4.

physical variables at their corresponding grid nodes in a simulation region can be obtained by CFD method. Here, after the solution of the governing equations of the flows, the value of velocity of fluid particles in motion at its corresponding velocity-grid point can be obtained, so that we can count the number of velocity-grid points with a velocity greater than 0.30 m/s, and then, a percentage of which to the number of the total velocity-grid points, *P*, can be obtained.

Here, under the 4 different submergence depth ratios 1/4, 1/3, 1/2, and 3/4 of the surface aerator, we take *P* as a statistical variable for analysis. The statistical variable, *P*, corresponding to its submergence depth ratio is plotted in Fig. 11.

At the same time, to consider the effect of the submergence depth ratio on the hydraulic characteristics of the OD, the average gas volume fraction was also statistically studied. Fig. 12 shows the air volume fractions with the 4 different submergence depth ratios 1/4, 1/3, 1/2, and 3/4 of the surface aerator.

It can be seen from Fig. 11 that the submergence depth ratios of the surface aerator have a certain impact on the overall flow velocity distribution in the OD. With the submergence depth ratio of 1/2, the percentage of the fluid particles with a velocity greater than 0.30m/s to the total fluid particles, *P*, is of 49.05%, followed by the submergence depth

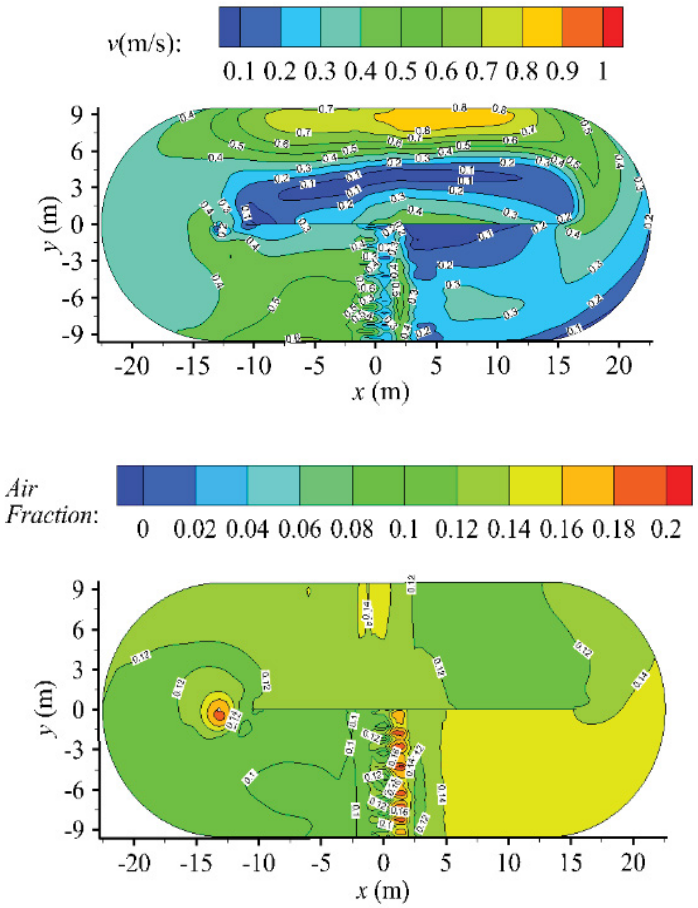

Fig. 10. Velocity and gas volume fraction distribution diagrams on the horizontal plane at z = 2.6 m: (a) velocity and (b) gas volume fraction.

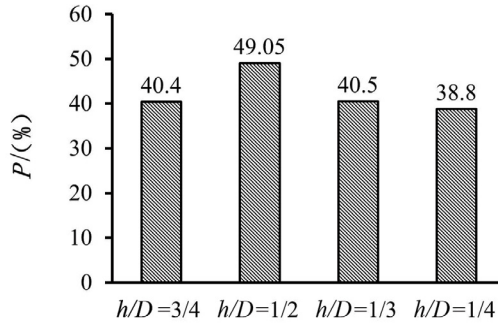

Fig. 11. Percentage of the fluid particles with a velocity greater than 0.3 m/s to the total fluid particles under the 4 different submergence depth ratios.

ratio 1/3 for 40.5%; and with the submergence depth ratios 3/4 and 1/4, P accounts for 40.4% and 38.8%, respectively.

As can be seen from Fig. 12, the gas volume fraction,19.6%, is the maximum corresponding to its submergence depth ratio of 1/3, followed by 15.3%, 12.9%, and 12.3%, which correspond to the submergence depth ratios of 1/2, 1/4, and 3/4, respectively. Therefore, only from the point of view in velocity, the submergence depth ratio 1/2 is the best one; but only from the point of view in the gas content, 1/3 should be the best one. Therefore, considering both the velocity distribution and the gas content, we proposed that the submergence depth ratio of the surface aerator ranges from 1/3 to 1/2 for the OD.

We can also draw the relationship curve in Fig. 13 describing the change of the cross-sectional averaged velocity in the straight ditch with the submergence depth ratio of the surface aerator, and then obtain its equation, $y = -138.86x^2 + 145.18x + 9.8852$, where x represents the submergence depth ratio (h/D), and y represents the average velocity over the cross-section. According to the equation, we obtained that, with x = 0.5, y reaches the maximum value of 0.39 m/s. Therefore, the submergence depth ratio of 1/2 is the best one among the others.

5. Some discussions and further study plan

Numerical simulation and experimental methods are dependent upon each other; experiment is the main way to investigate a new basic phenomenon, taking a large amount of observation data as the foundation, still, the validation for a numerical simulation result must use the measured (in a prototype or a model) data. Doing numerical simulation in advance can obtain the preliminary results,

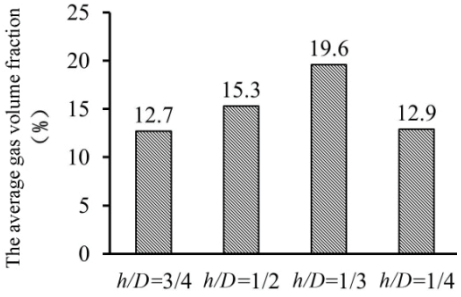

Fig. 12. Air volume fractions with the 4 different submergence depth ratios.

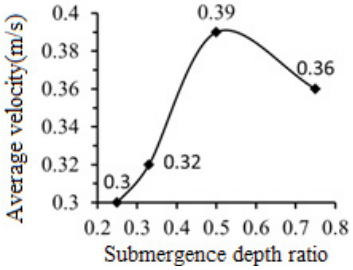

Fig. 13. The relationship curve of the cross-sectional averaged velocity and the submergence depth ratios.

which will make the corresponding experiment plan be more purposeful, and reduce the number of systematical experiments; therefore, it is much useful for the design of experimental device [11–13].

The submergence depth of surface aerator has effect on the structure of flow fields, aeration gas-volume-fraction distribution, and on the ability to move fluid in an OD, which needs to be studied by using experimental and CFD methods. In this paper, we used CFD method to compute the velocity fields and gas content distributions in an OD with the different submergence depth ratios, and obtained that the optimal submergence depth ratio ranges from 1/3 to 1/2 of the surface aerator. Further study will be done to validate the simulation model by an experimental method. An experimental model for the OD will be made of organic glass, according to the gravity similarity law (also named Froude number similarity theory) [14]. ADV will be used to measure velocities of the test model for the OD under the working conditions to validate the reliability of the simulation results.

6. Conclusions

The CFD technique with RNG k–ε turbulent model was used to simulate the flow velocity and gas content under different submergence depth ratios of the surface aerator in an OD, by which the conclusions are obtained as follows:

- with the submergence depth ratio of 1/3, the gas volume fraction near the bottom and the water surface in the OD was higher than that of the submergence depth ratios of 3/4, 1/2, and 1/4; and the velocity near the bottom increases, and near water surface decreases, which shows that the flow tends to be more uniform than that of the other submergence depth ratios. Therefore, the flow pattern with the submergence depth ratio of 1/3 is conducive to improving the processing ability of the OD and to reducing sludge deposition at OD bottom.
- with the submergence depth ratio of 1/2, the fluid particles of velocity greater than 0.30 m/s to the total fluid particles is of 49.05%, followed by the submergence depth ratio 1/3, accounting for 40.5%; with the submergence depth ratio of 1/3, the gas volume fraction 19.6% is the maximum, followed by gas volume fractions of 15.3% with the submergence depth ratio of 1/2. Therefore, considering the velocity distributions and the gas contents in a comprehensive way, we proposed that the optimal submergence depth ratio ranges from 1/3 to 1/2 for the OD.
- Numerical simulation is an effective method to study the hydraulic characteristics of an OD; the simulation results have a certain guiding significance for reducing sludge deposit in an actual project and improving efficiency of sewage treatment.

Acknowledgments

Financial support of this study was from the National Natural Science Foundation of China (Grant No.51578452 and No.51178391) and the scientific research projects of Shaanxi Province (2020SF-354, 2016GY-180, 2015slkj-08).

Symbols

C_μ — Model parameter in (4) with a value of 0.085
C_1 — Model parameter in (6)
C_2 — Model parameter in (6) with a value of 1.68
F_g — Volume fraction of gas
F_w — Volume fraction of liquid
g_i — Gravitational acceleration in i-direction, and i = 1, 2, and 3 m/s^2
k — Turbulent kinetic energy, m^2/s^2
p — Pressure, kg/m s^2
P — Percentage of grid points with velocity greater than 0.30 m/s
G_k — Production term in (5) and (6)
S — Parameter for computing C_1
$S_{i,j}$ — Parameter for computing C_1
t — Time, s
u_i — Velocity component in i-direction, and i = 1, 2, and 3 m/s
u_i' — Fluctuating velocity component in i-direction, and i = 1, 2, and 3 m/s
V_g — Volume of gas in a cell, m^3
V_c — Volume of a cell, m^3
V_w — Volume of liquid in a cell, m^3
v — Total velocity, m/s
x_i — Space coordinate in i-direction, and i = 1, 2, and 3 m

Greek

β — A constant of 0.015 for computing C_1
δ_{ij} — Kronecker function in (3), δ_{ij} = 1 with $i = j$, and δ_{ij} = 0 with $i \neq j$

ε — Kinetic energy dissipation rate, m^2/s^3
η — Parameter for computing C_1
η_0 — Constant of 4.38 for computing C_1
μ — Molecular kinematic viscosity, kg/m s
μ_t — Turbulent kinematic viscosity, kg/m s
ρ — Density, kg/m^3
σ_k — Model parameter in (5) with a value of 0.7197
σ_ε — Model parameter in (6) with a value of 0.7197

Subscripts

c — Cell
g — Gas
i,j — Direction, i = 1, 2, and 3; and j = 1, 2, and 3
t — Turbulence
w — Water

References

[1] L. Fan, N. Xu, Zh. Wang, H. Shi, PDA experiments and CFD simulation of a lab-scale oxidation ditch with surface aerators, Chem. Eng. Res. Des., 88 (2010) 23–33.
[2] W.-M. Xie, R. Zhang, W.-W. Li, B.-J. Ni, F. Fang, G.-P. Sheng, H.-Q. Yu, J. Song, D.-Z. Le, X.-J. Bi, C.-Q. Liu, M. Yang, Simulation and optimization of a full-scale Carrousel oxidation ditch plant for municipal wastewater treatment, Biochem. Eng. J., 56 (2011) 9–16.
[3] V. Diamantis, I. Papaspyrou, P. Melidis, A. Aivasidis, High aeration rate enhances flow stratification in full-scale oxidation ditch, Bioprocess Biosyst. Eng., 33 (2010) 293–298.
[4] B. Li, W. Cao, Research on improvement effects of brush aerator, Water Purif. Technol., 27 (2008) 67–69 (in Chinese).
[5] Z. Li, J. He, Y. Xu, H. Song, Characteristics of flow fields in oxidation ditches under action of aeration turntables, J. Hohai Univ. (Nat. Sci.), 39 (2011) 143–147 (in Chinese).
[6] Y. Yang, J. Yang, J. Zuo, Y. Li, S. He, X. Yang, K. Zhang, Study on two operating conditions of a full-scale oxidation ditch foroptimization of energy consumption and effluent quality by using CFD model, Water Res., 45 (2011) 3439–3452.
[7] L. Lei, J. Ni, Three-dimensional three-phase model forsimulation of hydrodynamics, oxygen masstransfer, carbon oxidation, nitrification anddenitrification in an oxidation ditch, Water Res., 53 (2014) 200–214.
[8] H. Xie, J. Yang, Y. Hu, H. Zhang, Y. Yang, K. Zhang, X. Zhu, Y. Li, C. Yang, Simulation of flow field and sludge settling in a full-scale oxidation ditch by using a two-phase flow CFD model, Chem. Eng. Sci., 109 (2014) 296–305.
[9] F. Dang, Sh. Zhang, Guide plate in the productive application of oxidation ditch, Liaoning Urban and Rural, Environ. Sci. Technol., 25 (2005) 29–31 (in Chinese).
[10] G. Chen, H. Zhao, J. Zhou, Study on flow characteristics of oxidation ditch with/without one-side guide wall, Energy Res. Manage., 4 (2010) 26–29 (in Chinese).
[11] W. Wei, X. Chen, W.L. Lou, Y. Cai, J. Wei, Y. Zheng, CFD method for the liquid–gas two-phase flow fields in an Orbal oxidation ditch, Desal. Water Treat., 126 (2018) 135–143.
[12] W. Wei, Y. Liu, B. Lv, Numerical simulation of optimal submergence depth of impellers in an oxidation ditch, Desal. Water Treat., 57 (2016) 8228–8235.
[13] W. Wei, Ch. Wang, J. Wei, Y. Cai, Y. Chang, B. Lv, Y. Hu, CFD for the influence of submergence depth of impellers on the flow field and sludge concentration distributions in an oxidation ditch, Desal. Water Treat., 201 (2020) 86–94.
[14] E.J. Finnemore, J.B. Franzini, Fluid Mechanics with Engineering Applications (10th ed.), McGraw-Hill Companies, Inc., New York, 2002.